Core hysteresis in nematic defects

Samo Kralj[1,2] and Epifanio G. Virga[3]
[1]*Laboratory of Physics of Complex Systems, Faculty of Education, University of Maribor, Koroška 160, 2000 Maribor, Slovenia*
[2]*Condensed Matter Physics Department, Jožef Stefan Institute, Jamova 39, 1000 Ljubljana, Slovenia*
[3]*Department of Mathematics, INFM Research Unit, University of Pavia, Via Ferrata 1, 27100 Pavia, Italy*
(Received 21 April 2002; published 6 August 2002)

We study field-induced transformations in the biaxial core of a nematic disclination with strength $m=1$, employing the Landau–de Gennes order tensor parameter **Q**. We first consider the transition from the defectless escaped radial structure into the structure hosting a line defect with a negative uniaxial order parameter along the axis of a cylinder of radius R. The critical field of the transition monotonically increases with R and asymptotically approaches a value corresponding to $\xi_b/\xi_f \approx 0.3$, where the correlation lengths ξ_b and ξ_f are related to the biaxial order and the external field, respectively. Then, in the same geometry, we focus on the line defect structure with a positive uniaxial ordering along the axis, surrounded by the *uniaxial sheath*, the uniaxial cylinder of radius ξ_u with negative order parameter and director in the transverse direction. We study the hysteresis in the position of the uniaxial sheath upon increasing and decreasing the field strength. In general, two qualitatively different solutions exist, corresponding to the uniaxial sheath located close to the defect symmetry axis or close to the cylinder wall. This latter solution exists only for strong enough anchorings. The uniaxial sheath is for a line defect what the *uniaxial ring* is for a point defect: by resorting to an approximate analytic estimate, we show that essentially the same hysteresis exhibited by the uniaxial sheath is expected to occur at the uniaxial ring in the core structure of a point defect.

DOI: 10.1103/PhysRevE.66.021703 PACS number(s): 61.30.Jf

I. INTRODUCTION

Though vastly explored, point and line defects in uniaxial nematic liquid crystals are still both fascinating and challenging [1,2]. They are often topologically or energetically stabilized in confined samples by constraints imposed on the surface [3,4]. Nematic defects, either points or lines, are conventionally classified into different classes according to their topological charge N, which in the director theory is always an integer (see, for example, Ref. [2] for a wide review). The charge of a point defect is obtained by examining the mapping of the nematic director field **n** on a closed surface surrounding the defect into the order parameter space, that is, the projective plane, since **n** and $-\mathbf{n}$ are equivalent. Such an equivalence ultimately makes the sign of N immaterial. For a line defect, often called a *disclination*, the strength m, which is half an integer, helps classifying different symmetries within the two possible topological classes (with $N=0$ and $N=1$, respectively): m is also defined as half the *Frank index*; it reflects the behavior of **n** on a loop encircling the line (see, specifically, p. 201 of Ref. [2]). However, close to the defect origin **n** is no longer sufficient to describe the molecular alignment: the fine structure of the defect core is more appropriately described by the order tensor **Q**, which comprises both uniaxial and biaxial states.

While the static structure of defects in the absence of external fields is rather well understood (as witnessed by the list of papers [6–14]), the effects produced on this structure by external fields are little studied [15,16]. Some experimental studies [16] reveal that strong fields can induce hysteresis in the defect core. To understand the basic features of these effects, we focus in this paper on the field-induced transformations in the biaxial core of both a disclination with $m=1$ and a radial *hedgehog*, the typical point defect with $N=1$.

The plan of the paper is as follows. In Sec. II we outline the model: in particular, we write the free energy (Sec. II A) and choose a special parametrization (Sec. II B), thus arriving at the corresponding Euler-Lagrange equations (Sec. II C). The nematic structures of interest and the core structures of both a disclination with $m=1$ and a radial hedgehog are compared in Sec. II D. The numerical results are presented in Sec. III: in Sec. III A, we study the field-induced transition between a defectless structure and a structure hosting a line defect; in Sec. III B, we focus attention on the hysteresis induced by the field in the core of a line defect; finally, in Sec. III C, we show a qualitative analogy between the hysteresis effects in the core of a line defect and those in the core of a point defect. Our main conclusions are then summarized in the last section.

II. MATHEMATICAL MODEL

A. Free energy

We describe nematic states through a symmetric and traceless order tensor **Q**. In its eigenframe it can be expressed as $\mathbf{Q}=\sum_{i=1}^{3} q_i \mathbf{e}_i \otimes \mathbf{e}_i$, where $\mathbf{e}_i$, for $i=1, 2, 3$, are the eigenvectors and q_i the corresponding eigenvalues [11,17]. In the uniaxial limit, **Q** reduces to $\mathbf{Q}=s(\mathbf{n}\otimes\mathbf{n}-\frac{1}{3}\mathbf{I})$, where **n** is the nematic director, s is the uniaxial scalar order parameter, and **I** is the identy tensor.

According to Ref. [18], the degree of biaxiality is defined as

$$\beta^2 = 1 - 6\frac{(\mathrm{tr}\,\mathbf{Q}^3)^2}{(\mathrm{tr}\,\mathbf{Q}^2)^3} \tag{1}$$

and ranges in the interval $[0,1]$. In all uniaxial states $\beta^2=0$, while states with maximal biaxiality correspond to $\beta^2=1$.

The free energy F stored in the region $\mathcal{B}$ occupied by the material can, in general, be expressed as the sum of two integrals,

$$F=\int_{\mathcal{B}}(f_{\mathrm{b}}+f_{\mathrm{e}}+f_{\mathrm{f}})dv+\int_{\partial\mathcal{B}}f_{\mathrm{s}}da, \tag{2}$$

where v and a are the volume and area measures, respectively, and f_{b}, f_{e}, f_{f}, and f_{s} represent the densities for the bulk, the elastic, the external field, and the surface energies. In the lowest order approximation and for small $\mathbf{Q}$ these densities read as [5,11,14]

$$f_{\mathrm{b}}=A\,\mathrm{tr}\,\mathbf{Q}^2-B\,\mathrm{tr}\,\mathbf{Q}^3+C(\mathrm{tr}\,\mathbf{Q}^2)^2, \tag{2a}$$

$$f_{\mathrm{e}}=L|\nabla\mathbf{Q}|^2, \tag{2b}$$

$$f_{\mathrm{f}}=-\frac{\Delta\chi}{2}\boldsymbol{\zeta}\cdot\mathbf{Q}\boldsymbol{\zeta}, \tag{2c}$$

$$f_{\mathrm{s}}=\frac{W}{2}\mathrm{tr}(\mathbf{Q}-\mathbf{Q}_{\mathrm{s}})^2. \tag{2d}$$

Here the material constants A, B, and C determine the degree of nematic ordering in undistorted bulk. The elastic term is modeled by a single nematic elastic constant L related to the average Frank elastic constant K by $K=4Ls^2$ [5]. For a positive external field anisotropy $\Delta\chi$, the external (electric or magnetic) field $\boldsymbol{\zeta}$, introduced in Eq. (2c), forces uniaxial nematic molecules along the direction where it is applied; for $\Delta\chi<0$, it tends to align them in a perpendicular direction. The surface anchoring term is weighted by the anchoring constant W; it enforces the nematic ordering described by $\mathbf{Q}_{\mathrm{s}}$.

We further adopt Lyuksyutov's constraint [19] (see also Refs. [9,11,14]), which reads as

$$\mathrm{tr}\,\mathbf{Q}^2=\frac{A}{2C}. \tag{3}$$

Consequently, any local distortion in the nematic ordering can only be produced by either reorienting the eigenvectors $\mathbf{e}_i$ of $\mathbf{Q}$ or by exchanging two of its eigenvalues q_i. Within this approximation, all distortions that would require melting of the nematic order, attained at $\mathbf{Q}=\mathbf{0}$, are avoided by entering biaxial states. This is a reasonable assumption as long as the material constant B is considerably smaller than both A and C, as is the case in a deep nematic phase [5].

B. Parametrization

The symmetry of the problem suggests the choice of a cylindrical co-ordinate system $\{\rho,\vartheta,z\}$. The unit vectors along the co-ordinate axes are denoted by $\{\mathbf{e}_\rho,\mathbf{e}_\vartheta,\mathbf{e}_z\}$. By Lyuksyutov's constraint (3), all admissible order tensors can be represented through the following parametrization [11,14]:

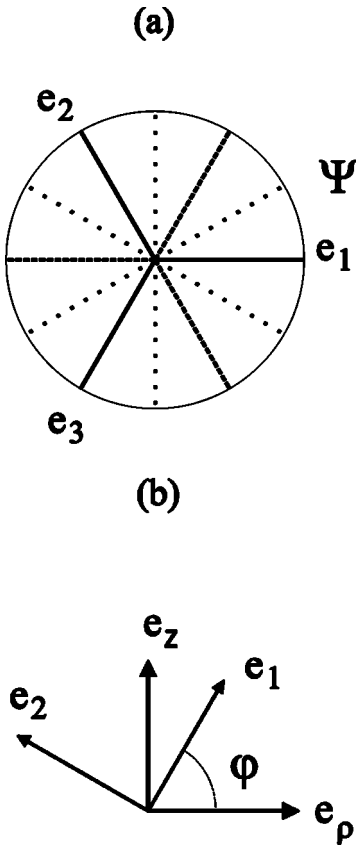

FIG. 1. (a) The nematic states described by the angle ψ. Full line: the uniaxial states with a positive eigenvalue and nematic director along $\mathbf{e}_i$ ($i=1$, $\psi=0$; $i=2$, $\psi=2\pi/3$; $i=3$, $\psi=-2\pi/3$). Dashed lines: uniaxial states with a negative eigenvalue and nematic director along $\mathbf{e}_i$($i=1$, $\psi=\pi$; $i=2$, $\psi=-\pi/3$; $i=3$, $\psi=\pi/3$). Dotted lines: states with maximal degree of biaxiality. (b) The co-ordinate system and the parametrization of the eigenvectors of $\mathbf{Q}$.

$$\mathbf{e}_1=\cos\varphi\mathbf{e}_\rho+\sin\varphi\mathbf{e}_z, \tag{4a}$$

$$\mathbf{e}_2=-\sin\varphi\mathbf{e}_\rho+\cos\varphi\mathbf{e}_z, \tag{4b}$$

$$\mathbf{e}_3=\mathbf{e}_\vartheta, \tag{4c}$$

$$q_1=\frac{2}{3}s_{\mathrm{eq}}\cos\psi,\quad q_2=-\frac{2}{3}s_{\mathrm{eq}}\cos\left(\psi+\frac{\pi}{3}\right),$$

$$q_3=-\frac{2}{3}s_{\mathrm{eq}}\cos\left(\psi-\frac{\pi}{3}\right). \tag{4d}$$

The equilibrium value s_{eq} of the uniaxial scalar order parameter is determined by Eq. (3), which can also be written as $\mathrm{tr}\mathbf{Q}^2=\frac{2}{3}s_{\mathrm{eq}}^2$. The angle ψ, which ranges in $[-\pi,\pi]$, describes the eigenvalues of $\mathbf{Q}$. As explained in detail in Refs. [11,14], it represents both uniaxial and biaxial states [Fig. 1(a)]. Moreover, the degree of biaxiality β^2 defined by Eq. (1) can be given an explicit representation in terms of ψ,

$$\beta^2=1-16\cos^2\psi\cos^2\left(\psi-\frac{\pi}{3}\right)\cos^2\left(\psi+\frac{\pi}{3}\right).$$

The angle φ determines the orientation of the eigenvectors of $\mathbf{Q}$ relative to the axes of the co-ordinate system [Fig. 1(b)]. It is indeed a merit of Lyuksyutov's constraint if only two scalars suffice to describe all admissible tensors $\mathbf{Q}$.

It is worth noting that this parametrization is not injective and there exist transformations in the parameter space that leave $\mathbf{Q}$ unchanged. The one that often plays a role in our study is

$$\mathbf{Q}(\varphi,\psi)=\mathbf{Q}\left(\varphi\pm\frac{\pi}{2},\frac{2\pi}{3}-\psi\right). \tag{5}$$

The reader is referred to Ref. [14] for more details.

The phenomena we are interested in describing involve structures that depend only on the co-ordinate ρ. This parametrization excludes twisted distortions that would make $\mathbf{Q}$ depend also on ϑ.

The region $\mathcal{B}$ that contains the material is here a cylinder of radius R. The lateral boundary of $\mathcal{B}$ weakly enforces the uniaxial homeotropic anchoring (it tends to align the nematic molecules along the surface normal). The external (electric or magnetic) field is aligned along the cylinder axis, that is, $\boldsymbol{\zeta}=\zeta\mathbf{e}_z$.

C. Scaled equilibrium equations

The characteristic lengths [5] entering this model are the biaxial correlation length $\xi_b=\sqrt{2L/3Bs_{eq}}$, the external field correlation length $\xi_f=\sqrt{4Ls_{eq}|\Delta\chi|\zeta^2}$, the surface extrapolation length $d_e=4L/W$, and the radius R of the confining cylinder. We measure all lengths relative to R so that $\rho\to R\rho$, $\xi_b\to R\xi_b$, $\xi_f\to R\xi_f$, $d_e\to Rd_e$, and $\nabla\to(1/R)\nabla$; in these units $R=1$. We measure the free energy F in terms of $F_0=RLs_{eq}^2$: thus, in the following $F\to F_0F$. For convenience, we also define the *excess free energy* as $\Delta F=F-F_{bulk}$, where F_{bulk} denotes the free energy of a nematic undistorted in bulk.

The dimensionless contributions to the excess free-energy density are expressed as

$$f_b=\frac{4}{27\xi_b^2}(1-\cos 3\psi), \tag{6a}$$

$$f_e=\frac{8}{3}\left[\frac{\psi'^2}{4}+\varphi'^2\sin^2\left(\psi-\frac{\pi}{3}\right)+\frac{\sin^2\left(\psi+\frac{\pi}{3}\right)\cos^2\varphi+\sin^2\psi\sin^2\varphi}{\rho^2}\right], \tag{6b}$$

$$f_f=\frac{\Delta\chi}{|\Delta\chi|}\frac{1}{3\xi_f^2}\left[\cos\left(\psi+\frac{\pi}{3}\right)\cos^2\varphi-\cos\psi\sin^2\varphi\right], \tag{6c}$$

$$f_s=\frac{1}{3d_e}[2+\cos\psi-\sqrt{3}\sin\psi+\cos^2\varphi(-3\cos\psi+\sqrt{3}\sin\psi)], \tag{6d}$$

where prime denotes differentiation with respect to ρ.

The corresponding bulk equilibrium equations are

$$0=-\rho^2\psi''-\rho\psi'+\frac{1}{3}\left(\frac{\rho}{\xi_b}\right)^2\sin 3\psi+2\left\{\sin\left[2\left(\psi-\frac{\pi}{3}\right)\right]\rho^2\varphi'^2+\sin\left[2\left(\psi+\frac{\pi}{3}\right)\right]\cos^2\varphi+\sin 2\psi\sin^2\varphi\right\}+\frac{\Delta\chi}{|\Delta\chi|}\frac{\rho^2}{4\xi_f^2}\left[-\sin\left(\psi+\frac{\pi}{3}\right)\cos^2\varphi+\sin\psi\sin^2\varphi\right], \tag{7a}$$

$$0=-2\left\{(\rho^2\varphi''+\rho\varphi')\sin^2\left(\psi-\frac{\pi}{3}\right)+\rho^2\sin\left[2\left(\psi-\frac{\pi}{3}\right)\right]\varphi'\psi'\right\}+\sin 2\varphi\left[\sin^2\psi-\sin^2\left(\psi+\frac{\pi}{3}\right)\right]-\frac{\Delta\chi}{|\Delta\chi|}\frac{\rho^2}{8\xi_f^2}\sin 2\varphi\left[\cos\left(\psi+\frac{\pi}{3}\right)+\cos\psi\right]. \tag{7b}$$

To avoid a singularity in Eq. (6b) at the cylinder axis, only the pairs

$$\{\varphi,\psi\}=\left\{0,\frac{2\pi}{3}\right\}\quad\text{and}\quad\{\varphi,\psi\}=\left\{0,-\frac{\pi}{3}\right\} \tag{7c}$$

are admissable. By Eq. (5) the same states are also represented by the pairs

$$\{\varphi,\psi\}=\left\{\frac{\pi}{2},0\right\}\quad\text{and}\quad\{\varphi,\psi\}=\left\{\frac{\pi}{2},\pi\right\}, \tag{7d}$$

respectively.

At the cylinder wall (where $\rho=1$) the following equations must be obeyed:

$$\psi'=\frac{1}{4d_e}[\sin\psi+\sqrt{3}\cos\psi-\cos^2\varphi(3\sin\psi+\sqrt{3}\cos\psi)], \tag{7e}$$

$$\varphi'\sin^2\left(\psi-\frac{\pi}{3}\right)=\frac{\sin 2\varphi}{16d_e}(-3\cos\psi+\sqrt{3}\sin\psi), \tag{7f}$$

which represent the appropriate boundary conditions for this variational problem where $\mathbf{Q}$ is not prescribed on the boundary. In the *strong anchoring* limit, that is, as $d_e\to 0$, both these conditions are to be replaced by the assignment of the parameters ψ and φ at $\rho=1$.

The above equilibrium equations have been solved numerically by using the over-relaxation method [20].

D. Nematic structures

In our study we consider nematic structures hosting line defects of strength $m=1$ along the cylinder axis. In our parametrization there are two qualitatively different structures of this type: the *planar radial* (PR) structures, with either a positive or negative scalar order parameter at $\rho=0$ [14]. Henceforth we denote them by PR_+ and PR_-, respectively. In both, the eigenvectors of **Q** are oriented along the axes of the cylindrical co-ordinate system: $\varphi_{\mathrm{PR}_\pm}\equiv 0$ in either PR structure. The uniaxial states at $\rho=0$ and $\rho=1$ (the latter strictly realized only in the strong anchoring limit) are attained through an *exchange* between the eigenvalues of **Q** [6,9]. In our parametrization, this is reflected by the function ψ which varies monotonically from $\psi_{\mathrm{PR}_\pm}(1)=0$ for either PR structure to $\psi_{\mathrm{PR}_+}(0)=2\pi/3$ and $\psi_{\mathrm{PR}_-}(0)=-\pi/3$, respectively. Thus, $\psi_{\mathrm{PR}_-}(\rho)$ crosses no uniaxial state in the interval $0<\rho<1$; it attains the maximum degree of biaxiality (corresponding to $\psi_{\mathrm{PR}_-}=-\pi/6$) at a distance $\rho=\rho_\mathrm{b}\approx\xi_\mathrm{b}$. Contrariwise, $\psi_{\mathrm{PR}_+}(\rho)$ crosses the uniaxial state with negative order parameter and nematic director along $\mathbf{e}_\vartheta$ at $\rho=\xi_\mathrm{u}$, where $\psi_{\mathrm{PR}_+}(\xi_\mathrm{u})=\pi/3$; in addition, the corresponding structure attains the maximum degree of biaxiality at $\rho=\rho_{\mathrm{b}1}$ and $\rho=\rho_{\mathrm{b}2}$, where $\psi_{\mathrm{PR}_+}(\rho_{\mathrm{b}1})=\pi/6$ and $\psi_{\mathrm{PR}_+}(\rho_{\mathrm{b}2})=\pi/2$, respectively. Moreover, $0<\rho_{\mathrm{b}1}<\xi_\mathrm{u}<\rho_{\mathrm{b}2}<1$. In our parametrization, $\rho_\mathrm{b}\approx 2\xi_\mathrm{b}$, $\rho_{\mathrm{b}1}\approx 1.6\xi_\mathrm{b}$, $\xi_\mathrm{u}\approx 2.3\xi_\mathrm{b}$, $\rho_{\mathrm{b}2}\approx 3.0\xi_\mathrm{b}$, for $R/\xi_\mathrm{b}>5$ [14]. We shall refer to the inner cylinder at $\rho=\xi_\mathrm{u}$ as the *uniaxial sheath*. Among the PR's only PR_- exhibits this feature, provided the extrapolation length d_e is sufficiently smaller than R.

Note that for large enough cavities and in the absence of any external field, either PR is metastable with respect to the defectless *escaped radial* (ER) structure, where the line defect is avoided by the escape of the director along the symmetry axis [21]: the angle φ here monotonically decreases from $\varphi_{\mathrm{ER}}(0)=\pi/2$ towards $\varphi_{\mathrm{ER}}(1)=0$. In the limit of strong homeotropic anchoring and in the approximation of equal Frank elastic constants, the ER solution is given by

$$\varphi_{\mathrm{ER}}(\rho)=\frac{\pi}{2}-2\arctan\rho, \tag{8a}$$

$$\psi_{\mathrm{ER}}(\rho)=0. \tag{8b}$$

In the absence of external fields, in the strong anchoring limit, and deep in the nematic phase (where melting of nematic ordering is avoided), the PR_- line defect structure can only be stable with respect to ER for small enough radii ($R/\xi_\mathrm{b}<11$, for the parameters in our model).

It is worth noting that the characteristic features of a disclination with strength $m=1$ and a radial hedgehog are similar in the plane where the exchange of eigenvalues takes place (henceforth referred to as the *defect plane*). These defects are schematically depicted In Figs. 2(a) and 2(b). The corresponding biaxial core structures in the defect plane are compared in Fig. 2(c): there the angles describing the evolution of **Q** exhibit qualitatively almost the same profile. In the core structure of a point defect the whole uniaxial sheath is replaced by a single *uniaxial ring* in the defect plane [9]: we shall treat below the uniaxial sheath and the uniaxial ring as essentially equivalent, though they appear in very different core structures. A reason for this will be given in Sec. III C.

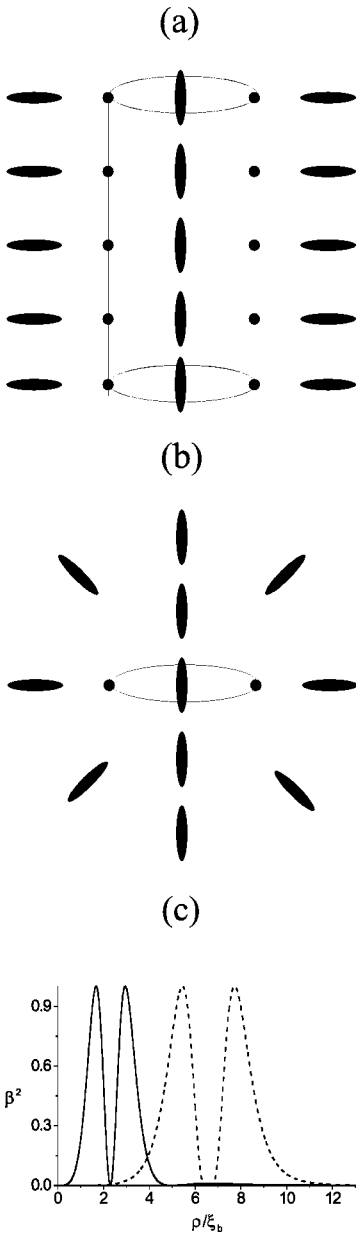

FIG. 2. Schematic presentation of a core structure in the (ρ,z) cross section for a disclination with strength $m=1$ (a) and for a radial hedgehog (b). A thin line indicates both the *uniaxial sheath* (a) and the *uniaxial ring* (b), where a negative nematic ordering is present with the director **n** in the azimuthal direction. Both at the defect origin and far from it the nematic ordering is uniaxial with a positive nematic order parameter. In (c) the biaxiality profiles of both the line defect (full line) and the point defect (dashed line) are compared in the *defect plane*, that is, the plane containing the uniaxial ring. Note that in the whole interval $0<\rho<R$, β^2 vanishes only at $\rho=\xi_\mathrm{u}$: $\xi_\mathrm{u}\approx 2.2\xi_\mathrm{b}$ and $\xi_\mathrm{u}\approx 6.5\xi_\mathrm{b}$ for the line and the point defect, respectively.

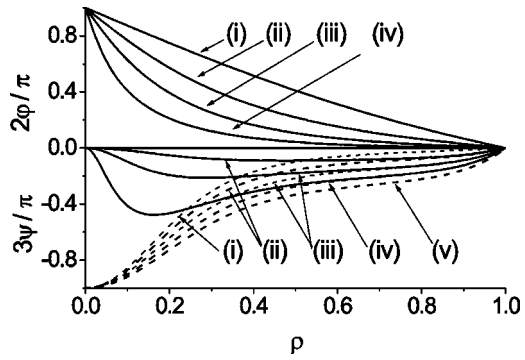

FIG. 3. The functions $\varphi(\rho)$ and $\psi(\rho)$ corresponding to ER (full line) and PR$_-$ (dashed line) for different external field strengths. (i) $\xi_b/\xi_f=0$, (ii) $\xi_b/\xi_f=0.3$, (iii) $\xi_b/\xi_f=0.6$, (iv) $\xi_b/\xi_f=0.9$, (v) $\xi_b/\xi_f=1.2$. Here $R/\xi_b=10$.

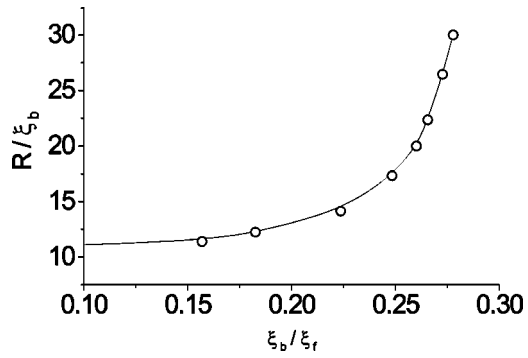

FIG. 5. Stability diagram of the pair of equilibrium solutions ER and PR$_-$ in the $(\xi_b/\xi_f,\ R/\xi_b)$ plane. The line is a guide for the eye.

III. NUMERICAL RESULTS

A. Field-induced PR$_-$ structure

We imagine to start without external fields from the ER solution in a large enough cavity $(R/\xi_b>10)$, where ER is stable with respect to PR$_-$. Then the external field $\boldsymbol{\zeta}=\zeta\mathbf{e}_z$ is applied to the nematic liquid crystal with $\Delta\chi<0$ filling the cilindrical cavity. The field would favor PR$_-$ tending to squeeze the nematic molecules in the $\{\mathbf{e}_\rho,\mathbf{e}_\vartheta\}$ plane. Upon increasing the field strength, the eigenvalues $q_1$and q_2 [Eqs. (4d)] approach each other driving the system into the PR$_-$ solution, as illustrated in Figs. 3 and 4.

In Fig. 3, the changes in both ER and PR$_-$ are shown for different values of ζ. For larger ζ's the director profile of ER approaches that of PR$_-$, and consequently the biaxiality of the structure becomes progressively larger. At the threshold field $\zeta=\zeta_c$, corresponding to $\xi_b/\xi_f^{(c)}\approx0.28$ for $R/\xi_b\gg10$, ER becomes metastable with respect to PR$_-$. Moreover, at even larger fields ER also ceases to exist. At a critical value $\zeta=\zeta_c^{(+)}$, corresponding to $\xi_b/\xi_f^{(+)}\approx0.95$, ER discontinuously transforms into PR$_-$. In this event, the main changes take place at the cylinder axis, where a positive uniaxial ordering transforms into a negative one. In our parametrization, this is reflected in changing the pair $\{\varphi(0),\psi(0)\}$ from $\{\pi/2,0\}$ to $\{0,-\pi/3\}$. The transition is clearly manifested in Fig. 4, where the minimum value of ψ for the ER structure is shown as a function of ξ_b/ξ_f, for different values of R. In the range $R/\xi_b>10$, the threshold condition is almost independent of R. In the same figure we also compare the averages taken over a sample volume of the degrees of biaxialities β^2_{ER} and $\beta^2_{PR_-}$ for ER and PR$_-$, respectively. Actually, the two degrees become identical above the threshold field $\zeta_c^{(+)}$.

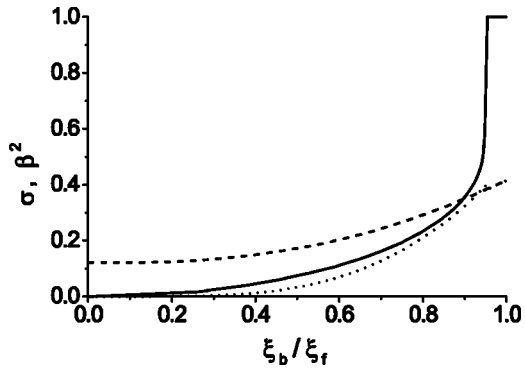

FIG. 4. The minimum value $\sigma=\min_{0\leq\rho\leq1}[-\psi_{ER}(\rho)/(\pi/3)]$ is plotted as a function of ξ_b/ξ_f (full line). In the same graph the average of β^2 is also shown for both ER (dotted line) and PR$_-$ (dashed line) structures. Here $R/\xi_b=10$.

In Fig. 5 we plot the stability diagram of the competition between ER and PR$_-$ as a function of both the cavity size and the external field strength. For $R/\xi_b\approx10.5$, the transition takes place at $\zeta=0$. For larger cavities, the threshold monotonically increases and eventually saturates at a critical value of ζ corresponding to $\xi_b/\xi_f^{(c)}\approx0.28$. For strong enough fields, for which $\xi_b/\xi_f^{(+)}\approx0.95$, the ER structure ceases to exist even as a metastable solution.

The field-induced transition ER-PR$_-$ separates qualitatively different equilibrium solutions satisfying the conflicting boundary conditions at $\rho=0$ and $\rho=1$. For $\zeta<\zeta_c$, this conflict is resolved by a rotation of the eigenframe of $\mathbf{Q}$, whereas for $\zeta\geq\zeta_c$ it is resolved by an exchange of the eigenvalues. Contrary to conventional Frederiks transitions [5], where the nematic uniaxial director field experiences a qualitative change, the threshold condition is here almost independent of R, provided this is large enough.

It is worth noting that the first order character of the ER-PR$_-$ transition anticipates an hysteresis in a real experiment. This phenomenon is discussed in more detail in the following section.

B. Field-induced hysteresis

We focus here on the PR$_+$ solution, which hosts a line defect of strength $m=1$ with a positive uniaxial ordering along the axis. We explore how the radius ξ_u of the uniaxial sheath depends on ζ for $\Delta\chi>0$. It should be noted that in the whole regime studied this structure is metastable with respect to both ER and PR$_-$. Nevertheless, it is worth studying because one can gain a qualitative understanding of the way a field affects the uniaxial sheath: this might be of interest for other experimentally accessible defect structures, as it will be shown below.

To this purpose we first explore in the strong anchoring limit how the excess free energy ΔF_{PR_+} of the PR$_+$ structure

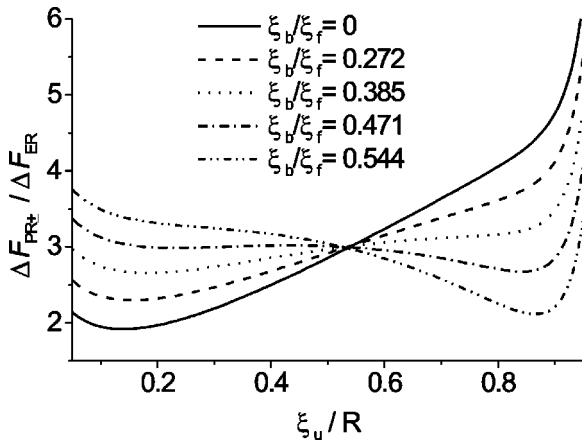

FIG. 6. The excess free energy ΔF_{PR_+} of PR_+ as a function of ξ_u for different external field strengths. Here $R/\xi_b = 5$. ΔF_{ER} is the excess free energy of ER.

depends on ξ_u, thought of as prescribed, for different values of ζ. For $\zeta = 0$, $\Delta F_{\mathrm{PR}_+}(\xi_u)$ exhibits a single minimum, as shown in Fig. 6. We refer to the solution corresponding to this minimum as the axial-PR_+ structure. In it the uniaxial sheath is close to the cylinder axis (over a distance comparable with ξ_b) to confine strong elastic distortions into a relatively small volume. The applied field tends to increase the central region of the defect, which is essentially uniaxial along the field direction. Consequently, for large enough external fields, precisely at $\zeta = \zeta_c^{(-)}$ (corresponding to $\xi_f = \xi_f^{(-)}$), the second minimum appears close to the cylinder wall (the distance $R - \xi_u$ is comparable with ξ_b): this is called the wall-PR_+ structure. Upon further increasing the external field, the relative difference between the two minima of the free energy decreases and it vanishes at a critical value $\zeta = \zeta_c$ (for which $\xi_f = \xi_f^{(c)}$), corresponding to a *Maxwell point*. At even larger fields, precisely at $\zeta = \zeta_c^{(+)}$ (for which $\xi_f = \xi_f^{(+)}$), the axial-PR_+ structure ceases to exist. Thus the axial-PR_+ solution exists for $\zeta \in [0, \zeta_c^{(+)}]$ and represents the global free-energy minimum for $\zeta \in [0, \zeta_c]$. Conversely, the wall-PR_+ solution exists for $\zeta \geq \zeta_c^{(-)}$ and represents the global free-energy minimum for $\zeta \geq \zeta_c$.

In a real experiment, upon increasing and decreasing the field strength a hysteresis is expected to appear in the dependence of ξ_u on ζ. To estimate the width of the hysteresis loop we henceforth assume that each equilibrium structure remains trapped in its local minimum as long as it exists.

In Fig. 7 the configurational changes in the core structure and the corresponding free energies are plotted as functions of the external field strength. The way ξ_u depends on ζ exhibits a pronounced hysteresis loop [Fig. 7(a)]. For increasing and decreasing external fields, the discontinuous transitions take place at $\mu_+ = \xi_b/\xi_f^{(+)} \approx 0.5$ and $\mu_- = \xi_b/\xi_f^{(-)} \approx 0.27$, respectively. The Maxwell point corresponds to $\xi_b/\xi_f^{(c)} \approx 0.3$, as can be inferred from the graph of ΔF_{PR_+} against ξ_u shown in Fig. 7(b). Note that with a good approximation ΔF_{PR_+} shows a linear dependence on $(\xi_b/\xi_f)^2$. This indicates that the field intervenes only through its direct contribution to the free-energy functional, while the changes it induces in the core structure are negligible, except at the discontinuous transitions. Thus, the core of both PR structures is essentially independent of ζ.

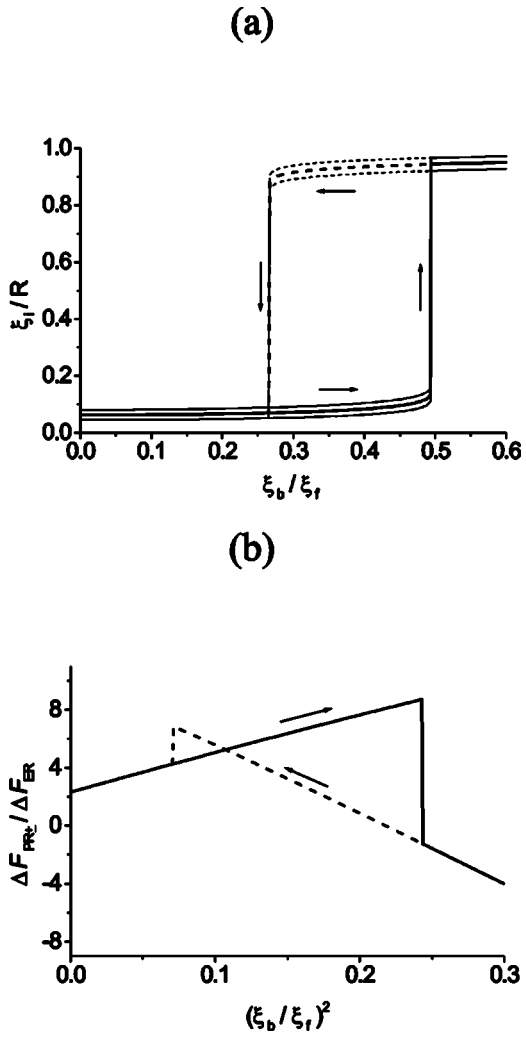

FIG. 7. (a) The typical lengths characterizing the defect core structure and (b) the excess free energy ΔF_{PR_+} of PR_+ as functions of ξ_b/ξ_f. ΔF_{ER} is the excess free energy of ER. In (a) ξ_i stands for ρ_{b1}, ξ_u, ρ_{b2} with $\rho_{b1} < \xi_u < \rho_{b2}$. Here $R/\xi_b = 35$.

The hysteresis shown in Figs. 6 and 7 is studied in a relatively large cavity ($R \approx 35\xi_b$). In Fig. 8 we show the influence of the cavity size on the hysteresis. One sees in Fig. 8(b) that the value of $\mu_+ \approx 0.5$ is essentially independent of R while μ_- monotonically decreases upon increasing R. In large cavities μ_- saturates at $\mu_- \approx 0.1$ and it merges with μ_+ for small enough cavities (for $R < R_c \approx 10\xi_b$). Therefore, below the critical radius R_c the hysteresis disappears and ξ_u depends smoothly on ζ when the external field is increased. Moreover, the jumps in ξ_u at the threshold field, defined by

$$\Delta\xi_u^{(\pm)} = \lim_{\delta\zeta \to 0^+} [\xi_u(\zeta^{(\pm)} + \delta\zeta) - \xi_u(\zeta^{(\pm)} - \delta\zeta)],$$

exhibit a linear dependence on R/ξ_b for $R > R_c$ [see Fig. 8(c)]. In addition, $\Delta\xi_u^{(+)} \approx \Delta\xi_u^{(-)}$ to within the experimental error. This suggests that the absolute position in space of the

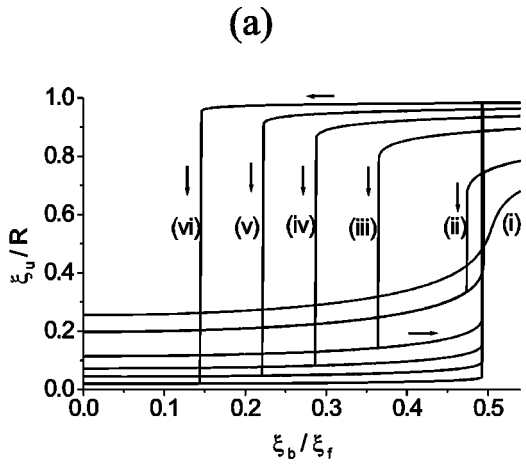

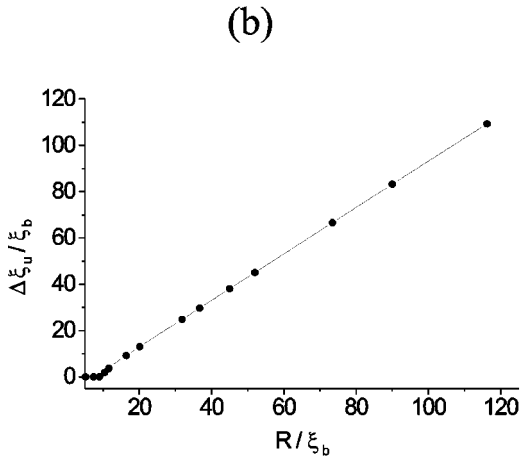

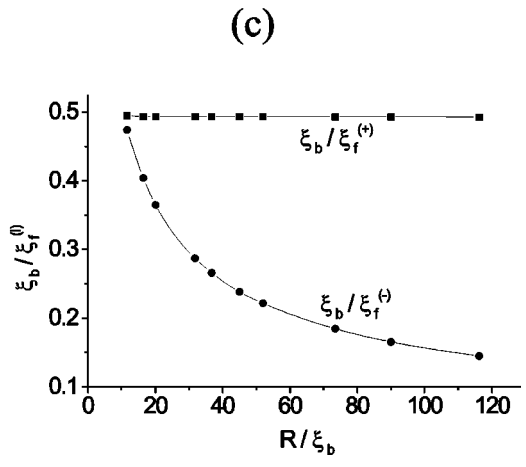

FIG. 8. Field-induced hysteresis for different values of R. The hysteresis disappears for $R/\xi_b \approx 10$. (a) $\xi_u = \xi_u(\zeta)$ for (i) $R/\xi_b = 9$, (ii) $R/\xi_b = 12$, (iii) $R/\xi_b = 20$, (iv) $R/\xi_b = 30$, (v) $R/\xi_b = 50$, (vi) $R/\xi_b = 120$. (b) $\Delta\xi_u^{(+)} \approx \Delta\xi_u^{(-)}$ as a function of R/ξ_b. (c) $\mu_- := \xi_b/\xi_f^{(-)}$ and $\mu_+ := \xi_b/\xi_f^{(+)}$ as functions of R/ξ_b.

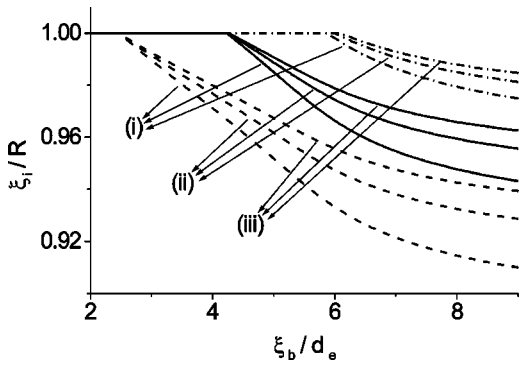

FIG. 9. The typical lengths ξ_i characterizing the defect core structure as functions of the anchoring strength. Dashed line, $\xi_i = \rho_{b1}$; full line, $\xi_i = \xi_u$; dash-dotted line, $\xi_i = \rho_{b2}$. (i) $R/\xi_b = 25$, (ii) $R/\xi_b = 30$, (iii) $R/\xi_b = 35$.

uniaxial sheath in both PR_+ equilibrium solutions is essentially independent of ζ as long as $R > R_c$.

The wall-PR_+ solution exists only for strong enough anchorings. When the anchoring is too weak the defect core virtually moves out of the cylinder. To demonstrate this we calculate the characteristic core radia ρ_{b1}, ξ_u, ρ_{b2} in terms of the anchoring strength, starting from the externally stabilized wall-PR_+ solution. The corresponding gradual disappearance of the core is shown in Fig. 9. Note that the critical anchoring strength shows a very weak dependence on R for $R > R_c$. The threshold value for the escape of the uniaxial sheath is given by $d_e \approx 0.25\xi_b$.

C. Hysteresis in the point defect core structure

In Sec. II D we remarked a qualitative similarity between the core structure of a disclination with strength $m = 1$ (PR_+) and that of a radial hedgehog, though only in the defect plane. In the following we estimate how the excess free energy ΔF_{PD} of the point defect depends on the ring radius ξ_u. We imagine the point defect as being confined within a sphere with radius R, and the external field ζ applied along the defect symmetry axis $\mathbf{e}_z$. We show that the function $\xi_u \mapsto \Delta F_{PD}$ exhibits a behavior qualitatively similar to the one studied in the preceding section.

To find an approxiamte analytic expression for ΔF_{PD}, we imagine the following representation of the defect core structure for an arbitrary field strength ζ [14,22]. It basically consists of three different regions, which we label by I, II, and III as shown in Fig. 10. The central region I is a sphere of radius $r = \xi_u$ where the nematic ordering is uniaxial and homogeneously aligned along $\mathbf{e}_z$. Near the defect plane, region I is surrounded by the torus where the biaxiality is the highest [14]: this is the region where the exchange of eigenvalues takes place. Region II is further surrounded by the radially oriented uniaxial nematic director field for $r > \xi_u$. Thus, in our parametrization, $\psi = 0$ in both regions I and III. In region II, a stepwise function is taken for $\psi(\rho)$,

$$\psi|_{\xi_u \geqslant \rho \geqslant \xi_u - (\Delta\rho/2)} = \frac{2\pi}{3\Delta\rho}\left(\rho - \xi_u + \frac{\Delta\rho}{2}\right)$$

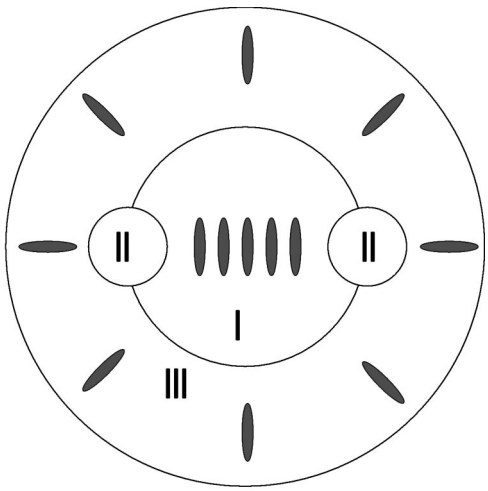

FIG. 10. Schematic representation of the point defect structure used in deriving Eq. (9). In I the nematic ordering is uniaxial and uniformly aligned. In II the order is biaxial; this is the region where the exchange of eigenvalues takes place. In III the nematic ordering is uniaxial and oriented radially.

and

$$\psi|_{\xi_u+(\Delta\rho/2)\geqslant\rho\geqslant\xi_u}=\frac{2\pi}{3\Delta\rho}\left(-\rho+\xi_u+\frac{\Delta\rho}{2}\right),$$

where $\Delta\rho=k\xi_b$ (with $k\approx 2$) is the radius of the torus in region II (in a cavity large enough with respect to ξ_b [22]). We also need to estimate the director field derivative in passing from region I to region III [22]. This contribution to the free energy becomes important for a relatively large field ζ, where the uniaxial ring is squeezed near the surface. We assume that the radial derivative of the angle describing the director field is approximately $1/(R-\xi_u)$, where $R-\xi_u$ is the width of region III.

With this picture in mind, after integration over the whole sphere of radius R, one gets

$$\frac{\Delta F_{PD}(\xi_u)}{2\pi}=16(1-\xi_u)-\frac{2\xi_u^3}{9\xi_f^2}+4k^2\pi\xi_u\xi_b^2\left[\frac{8}{27\xi_b^2}\left(1+\frac{4\pi^2}{k^2}\right)+\frac{2}{\xi_u^2}-\frac{1}{6\xi_f^2}\right]+\frac{2\xi_u^2}{1-\xi_u},\tag{9}$$

with the scaling introduced in Sec. II C.

For large enough radii ($R/\xi_b>10$), this function exhibits a single minimum close to the defect axis for weak enough fields. For stronger external fields, two minima appear, the second one corresponding to the ring located close to the sphere surface. For $R/\xi_b=20$, the minimum corresponding to the wall-PR_+ structure appears for $\xi_b/\xi_f\approx 1.2$ and the Maxwell point occurs at $\xi_b/\xi_f\approx 1.5$, while the first minimum disappears at $\xi_b/\xi_f\approx 2$. A characteristic plot is shown in Fig. 11.

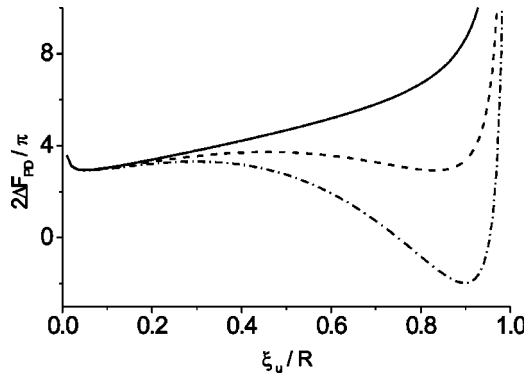

FIG. 11. The excess free energy ΔF_{PD} of a point defect (radial hedgehog) as a function of ξ_u for different ratios ξ_b/ξ_f. Full line, $\xi_b/\xi_f=0$; dashed line, $\xi_b/\xi_f=14$; dotted line; $\xi_b/\xi_f=20$. Here $R/\xi_b=20$.

IV. CONCLUSIONS

We studied the phenomena induced by an external field in the biaxial core of a nematic disclination with strength $m=1$ within the Landau–de Gennes approach, which employs the order tensor **Q** to describe the nematic molecular alignment. To simplify the analysis of the problem we resorted to Lyuksyutov's constraint [19]. Consequently, the melting of nematic ordering is prohibited and relatively strong nematic elastic distortions are resolved by entering biaxial states. Therefore, the approximation used is acceptable only for deep nematic phases.

In most of the study we explored transformations induced by an external field in the core of a cylinder with radius R. Thus, only the escaped radial (ER) and the planar radial structures with positive (PR_+) and negative (PR_-) uniaxial order parameter at the cylinder axis are competing for a minimum of the free energy. ER is stable with respect to both PR's for $\zeta=0$ and R large enough. We first considered the discontinuous transition of ER into PR_- that can be observed for materials with negative field anisotropy $\Delta\chi$. At a critical field ζ_c, which in large cavities corresponds to $\xi_b/\xi_f^{(c)}\approx 0.27$, a qualitative change in the tensor field **Q** takes place. For $\zeta<\zeta_c$, **Q** varies in space by rotating its eigenframe, whereas for $\zeta>\zeta_c$ it varies by exchanging its eigenvalues. The ER structure ceases to exist at $\xi_b/\xi_f^{(+)}\approx 0.95$ where it discontinuously transforms into PR_-. In real experiments, a hysteresis is expected because of the first order character of this transition. On increasing ζ, ER should persist until the condition $\xi_b/\xi_f^{(+)}\approx 0.95$ is met. Then, on reducing ζ, the nematic structure might remain trapped into PR_- until $\zeta=0$.

We next focused on the field-induced changes in the PR_+ structure. This equilibrium solution is characterized by the *uniaxial sheath* with a negative uniaxial ordering located at a distance ξ_u from the defect symmetry axis. We referred to the two possible PR_+ solutions in the external field as the axial-PR_+ and the wall-PR_+. The competition between the elastic and field energies decides whether the uniaxial sheath is placed close to the cylinder axis (axial-PR_+) or close to the wall (wall-PR_+); it can even be pushed out of the cylin-

der (if $d_e < 0.25\xi_b$). For weak enough fields, only the axial-PR$_+$ solution exists; conversely, for large enough fields, only the wall-PR$_+$ solutions exists, provided the anchoring strength is sufficiently large. The critical fields for the stability of these structures are represented by the ratios $\mu_+ = \xi_b/\xi_f^{(+)}$ and $\mu_- = \xi_b/\xi_f^{(-)}$, respectively. For large enough cavities ($R/\xi_b \gg 10$), these ratios saturate (i.e., they become independent of R) at $\mu_+ \approx 0.5$ and $\mu_- \approx 0.1$. Upon decreasing R, the values of μ_+ and μ_- gradually approach each other and finally merge at $R \approx 10\xi_b$. Note that these values determine the stability limits of the structures involved. Experimentally, one would actually observe a narrower hysteresis, the width of which depends on the ''noise'' in the system.

We have also shown that a similar field-induced hysteresis is expected to take place within a radial hedgehog. Thus, we represented the core structure of this point defect in an external field through an approximate model. This model confirmed qualitatively the picture we arrived at in the detailed study of the line defect. Our conclusion has also an experimental counterpart (see Ref. [16], where a strong field-induced hysteresis was observed).

In a future study we will consider the annihilation between the biaxial structures of a radial and a *hyperbolic* hedgehog (both point defects in the topological class with $N=1$). The annihilation can proceed without melting, displaying only changes in the biaxial spatial arrangement. In this study we will particularly focus on the post collision regime, where the core structure of the interacting defects gradually becomes indistinguishable.

ACKNOWLEDGMENTS

This research was supported by a bilateral cooperation between Slovenia and Italy and ESF network Project No.CO-SLAB.

[1] H. R. Trebin, Liq. Cryst. **24**, 127 (1998), and references therein.
[2] M. V. Kurik and O. D. Lavrentovich, Sov. Phys. Usp. **31**, 196 (1988) [Usp. Fiz. Nauk **154**, 381 (1988)], and references therein.
[3] N. D. Mermin, Rev. Mod. Phys. **51**, 591 (1976).
[4] M. Kleman, *Points, Lines and Walls* (Wiley, Chichester, 1983).
[5] P. G. de Gennes and J. Prost, *The Physics of Liquid Crystals* (Oxford University Press, Oxford, 1993).
[6] N. Schopohl and T. J. Sluckin, Phys. Rev. Lett. **59**, 2582 (1987).
[7] N. Schopohl and T. J. Sluckin, J. Phys. (France) **49**, 1097 (1988).
[8] S. Kralj, S. Žumer, and D. W. Allender, Phys. Rev. A **43**, 2943 (1991).
[9] E. Penzenstadler and H. R. Trebin, J. Phys. (France) **50**, 1025 (1989).
[10] E. M. Terentjev, Phys. Rev. E **51**, 1330 (1995).
[11] R. Rosso and E. G. Virga, J. Phys. A **29**, 4247 (1996).
[12] O. D. Lavrentovich, T. Ishikawa, and E. M. Terentjev, Mol. Cryst. Liq. Cryst. **299**, 301 (1997).
[13] E. C. Gartland and S. Mkaddem, Phys. Rev. E **59**, 563 (1999).
[14] S. Kralj, E. G. Virga, and S. Žumer, Phys. Rev. E **60**, 1858 (1999).
[15] S. Kralj and S. Žumer, Phys. Rev. A **45**, 2461 (1992).
[16] V. G. Bodnar, O. D. Lavrentovich, and V. M. Pergamenshchik, Zh. Éksp. Teor. Fiz. **101**, 111 (1992) [Sov. Phys. JETP **47**, 61 (1992)].
[17] P. Biscari and E. G. Virga, Int. J. Non-Linear Mech. **32**, 337 (1997).
[18] P. Kaiser, W. Wiese, and S. Hess, J. Non-Equilib. Thermodyn. **17**, 153 (1992).
[19] I. F. Lyuksyutov, Zh. Eksp. Teor. Fiz. **75**, 358 (1987) [Sov. Phys. JETP **48**, 178 (1987)].
[20] F. J. Vesely, *Computational Physics* (Plenum, New York, 1994).
[21] C. Williams, P. Pieranski, and P. E. Cladis, Phys. Rev. Lett. **29**, 90 (1972).
[22] S. Kralj and E. G. Virga, J. Phys. A **34**, 829 (2001).